INTERNATIONAL JOURNAL FOR NUMERICAL METHODS IN FLUIDS, VOL. 15, 1059–1071 (1992)

TURBULENCE MODELLING FOR DEEP OCEAN RADIONUCLIDE DISPOSAL

YASUO ONISHI AND DONALD S. TRENT
Pacific Northwest Laboratory, Richland, WA 99352, U.S.A.

SUMMARY

In this study the adequacy of the k–ε turbulence model and the feasibility of the three-dimensional hydrodynamic-transport models TEMPEST and FLESCOT for deep ocean radionuclide disposal assessment were evaluated qualitatively. TEMPEST and FLESCOT were applied to a hypothetical, two-dimensional, deep ocean case with and without stratifications. TEMPEST with the k–ε model was applied to obtain quasi-steady state eddy viscosity distributions. With calculated eddy viscosity distributions as part of the input, FLESCOT then calculated distributions of velocity, water temperature, sediment and the disssolved and sediment-sorbed radionuclide, assuming that the radionuclide was disposed on the ocean bottom.

Results revealed that the computed eddy viscosity increased almost linearly with vertical distance near the ocean bottom, then rapidly decreased towards a molecular viscosity value when the vertical gradient of the velocity distribution became very small. The results also demonstrate the importance of the density gradient to suppress the turbulent kinetic energy production, resulting in reduced eddy viscosity, producing the maximum computed eddy viscosity of 0·2 Pa s, which compares well with the reported value of 0·07 Pa s in the deep ocean. Thus the k–ε turbulence model appears to be qualitatively applicable to the deep ocean environment.

KEY WORDS Turbulence model Deep ocean Radionuclide Three-dimensional modelling Eddy viscosity

INTRODUCTION

Evaluations of deep ocean disposal of contaminants (e.g. radionuclides and toxic chemicals) must address both potential regional-scale impacts to the public and the marine environment along an adjacent coastline as well as potential long-term impacts to the general public and the marine environment on the global scale. These assessments require the understanding of how such contaminants migrate in the ocean on both regional and global scales.

This study addresses the regional-scale modelling as part of the U.S. Environmental Protection Agency's long-term effort to address the concerns of low-level radioactive waste (LLW) deep ocean disposal at the 2800 and 3800 m sites in the mid-Atlantic Ocean.

The LLW released from these sites will not reach its uniform distributions in either the vertical or horizontal direction on a regional scale (e.g. up to several hundred square kilometres) and the physical oceanographic properties exhibit complex three-dimensional behaviour.[1] Thus three-dimensional, coupled hydrodynamic-mass/energy transport models with proper representations of ocean eddy viscosity/dispersion processes and sediment–radionuclide interactions are required for regional radionuclide transport modelling.

0271–2091/92/211059–13$11.50

Received March 1992

Projections of basin-wide and global circulations, Gulf Stream meanders and worm-core rings, topographic Rossby waves as well as other large-scale flow and wave phenomena cannot be generated by regional models. Rather, the flow and property distributions resulting from such large-scale transport mechanisms must be imposed on the regional models as initial and boundary conditions. Thus one of the key processes that regional models must internally simulate is the deep ocean turbulence to reproduce proper flow and transport in the deep ocean.

After reviewing 24 representative mathematical models for the LLW ocean disposal assessment,[1] the three-dimensional hydrodynamic-transport models TEMPEST[2] and FLESCOT[3] containing the k–ε turbulence model[4] were applied to a two-dimensional deep rectangular basin to qualitatively examine applicabilities of the k–ε turbulence closure model and the TEMPEST and FLESCOT models to the potential deep ocean environment.

MODEL DESCRIPTION

The TEMPEST model is an unsteady, three-dimensional, finite difference hydrothermal model cast in Cartesian and cylindrical co-ordinates and is based on the conservation of

(i) fluid mass (equation of continuity)
(ii) momentum (the Navier–Stokes equations)
(iii) turbulent kinetic energy and its dissipation based on the k–ε model
(iv) thermal energy
(v) mass of constituents.

The model has an option for either iterative dynamic pressure calculation or hydrostatic pressure calculation. For the dynamic pressure calculation, all inertia and viscosity terms are retained in addition to the pressure and gravitational terms in the vertical component of the Navier–Stokes equations. The model can also simulate a free surface or rigid lid at the water surface.

The FLESCOT model is the sediment and contaminant transport version of the general code TEMPEST and includes additional mass transport equations for

(i) mass of sediment
(ii) mass of dissolved contaminant
(iii) mass sediment-sorbed contaminants.

Sediments and sediment-sorbed contaminants are modelled separately for three sediment size fractions (usually sand, silt and clay fractions). The model uses the Partheniades[5] and Krone[6] formulae to estimate cohesive sediment erosion and deposition. The DuBoy[7] formula is used to estimate non-cohesive sediment erosion and deposition. The model can accommodate wave-enhanced sediment and sediment-sorbed contaminants by imbedding the non-linear Grant–Madsen flow–wave interaction model.[8] An exchange of a contaminant between water and sediment is modelled by assigning an equilibrium distribution coefficient (K_d) and an associated rate constant for each of the three sediment size fractions. The FLESCOT model also calculates changes of the sediment and sediment-sorbed contaminants within the multilayered seabed resulting from sediment erosion/deposition, bioturbation and direct adsorption/desorption between bottom sediment and overlying water.

The TEMPEST and FLESCOT models use a finite volume, time-marching procedure to simulate the three-dimensional, time-dependent, turbulent flow. This procedure advances the solution sequentially in two phases.

Phase I. Hydrodynamic solution

The hydrodynamic solution is advanced a time step Δt using one of the following three approaches:

(1) rigid lid (may be stationary or moving vertically according to tidal data)
(2) free surface with dynamic pressure (deep water wave theory)
(3) free surface with hydrostatic pressure (shallow water wave theory).

This phase computes the three velocity components u, v and w and the pressure field P at the new time level $t+\Delta t$.

The rigid lid approach requires computing the dynamic pressure field. This is accomplished using a 'semi-implicit' technique, which in TEMPEST is similar to the SMAC method developed at the Los Alamos National Laboratory.[9] This procedure is implemented as follows.

Step 1. Provisional velocity field computation (explicit). Compute a provisional velocity field, u, v and w, explicitly according to the momentum equations using pressures computed from the previous time step.
Step 2. Velocity and pressure field correction (implicit). The provisional velocity field found in Step 1 is then used to compute a provisional flow field divergence. A velocity and pressure field correction is then applied that causes the divergence of the flow to vanish, which must be the case for incompressible flow. Using these correction values, the new time velocity components u, v and w and the pressure field P are established.

Phase II. Transport solution

Once Phase I of the process has been completed, the new time velocity field is used to compute the scalar transport equations for thermal energy, T (if required), turbulent kinetic energy k and dissipation of turbulent kinetic energy, ε.

Once these quantities are computed, the new time eddy viscosity μ_T is established using the Prandtl–Kolmogorov hypothesis

$$\mu_T = C_\mu \rho k^2/\varepsilon, \tag{1}$$

where C_μ is a constant, assigned to be 0·09, and ρ is the water density.

Using the new time values of velocities and turbulent viscosity, the time step is completed by computing the constituent transport C_i (sediments and chemical species) and the new water density ρ.

This series of steps completes one time step, advancing all quantities to the new time level $t+\Delta t$. The process now returns to Step 1 of Phase I to start advancement to the next time level.

Differencing procedures

TEMPEST uses first-order upwind differencing procedures to discretize the inertial terms in the hydrodynamic equations and the advective terms in the scalar transport equations. Second-order-accurate central differencing procedures are used, as appropriate, for all other differential quantities. It is recognized that the upwind method produces a certain amount of numerical diffusion. In spite of this difficulty, the upwind method produces conservative and bounded results and avoids a variety of other erratic characteristics, including generation of false sources and sinks, associated with higher-order methods.

MODEL APPLICATIONS

To examine the k–ε model and radionuclide transport modelling in the deep ocean environment, TEMPEST and FLESCOT were applied to a two-dimensional rectangular basin 12000 m long and 3000 m deep. The model area was discretized by a rectangular grid having uniform grid spacing (500 m each) for the longitudinal direction and non-uniform grid spacing for the vertical direction with spacing of 0·1 m near the bottom. The ocean bottom was divided into four bed layers with a top layer 3 cm thick.

To predict the flow and radionuclide transport, the following modelling was performed.

1. The TEMPEST model was first applied to obtain the quasi-steady state vertical eddy viscosity by solving for hydrodynamics, water temperature and turbulence (the turbulence kinetic energy and its dissipation) under two sets of stratification (non-isothermal) cases and one non-stratification case. Salinity was assumed to be 32 parts per thousand for all cases. These conditions are shown in Table I. As indicated in Table I, two thermoclines were assumed for Cases 2 and 3, one near the water surface and the other near the ocean bottom. Note that Case 2 has the near-bottom thermocline at 120–150 m above the ocean bottom, while Case 3 has the near-bottom thermocline at only 6·0–7·5 m above the ocean bottom. For all three cases TEMPEST used the dynamic pressure calculation and the rigid lid options. As in the following radionuclide transport cases, the eddy viscosity and associated dispersion coefficients at each computational cell were assigned as

$$\text{vertical eddy viscosity} = \text{molecular viscosity} + \text{computed eddy viscosity by the } k\text{–}\varepsilon \text{ model}, \tag{2}$$

$$\text{longitudinal eddy viscosity} = \text{molecular viscosity} + \text{computed eddy viscosity} + \text{oceanographic horizontal eddy viscosity}. \tag{3}$$

In this study the oceanographic horizontal eddy viscosity was assumed to be 1000 Pa s. The non-isotropic dispersion coefficients were estimated by the corresponding eddy viscosity and the Schmidt/Prandtl numbers, which were assumed to be 0·71. The bottom drag coefficient was assigned to be 0·0026. To obtain the quasi-steady state eddy viscosity, TEMPEST was run for two simulated days.

2. Using the quasi-steady state eddy viscosity distribution obtained from the above TEMPEST runs, FLESCOT was then applied to calculated early distributions of flow, water temperature, sediments (sand, silt and clay) and radionuclides (both dissolved and

Table I. Initial and upstream boundary conditions for water temperature, salinity and velocity distributions

Distance from bottom (m)	Water temperature (° C)			Salinity (‰) All cases	Velocity (m s^{-1}) All cases
	Case 1	Case 2	Case 3		
2960–3000	10	16	16	32	0·1
2940–2960	10	13	13	32	0·1
150–2940	10	10	10	32	0·1
120–150	10	6	10	32	0·1
7·5–120	10	2	10	32	0·1
6·0–7·5	10	2	6	32	0·1
0–6·0	10	2	2	32	0·1

Table II. Selected values of sediment transport parameters

Sediment type	Sedilment diameter (m)	Fall velocity ($m\ s^{-1}$)	Critical shear stress for erosion ($N\ m^{-2}$)	Critical shear stress for deposition ($N\ m^{-2}$)	Erodability coefficient ($kg\ m^{-2}\ s^{-1}$)
Sand	$2{\cdot}5 \times 10^{-3}$	5×10^{-3}	—	—	—
Silt	$1{\cdot}6 \times 10^{-5}$	5×10^{-6}	0·045	0·02	4×10^{-6}
Clay	$2{\cdot}0 \times 10^{-6}$	1×10^{-6}	0·060	0·01	4×10^{-6}

sediment-sorbed) for Cases 1 and 2. In these cases the hydrostatic pressure and free surface options were used. For these cases bottom sediments were assumed to be 20% sand, 60% silt and 20% clay. It was also assumed that there were no radionuclides in the water column initially and that the radionuclides originally existed only in the bottom sediments of the 500 m reach between 1500 and 2000 m from the upstream end of the model area. The initial radionuclide concentrations associated with these bottom sediments were assumed to be 0·001, 1·0 and 5·0 $mCi\ g^{-1}$ for bottom sand, silt and clay respectively. Table II shows the sediment transport parameter values. The distribution coefficients K_d associated with sand, silt and clay were assigned to be 0·02, 20 and 100 $cm^3\ g^{-1}$ respectively. FLESCOT was run for 6 h.

MODEL RESULTS AND DISCUSSIONS

Turbulence modelling

TEMPEST was run for two simulated days to obtain quasi-steady state eddy viscosity distributions. All three cases indicate the highest values of turbulent kinetic energy (TKE) and TKE dissipation occurred near the ocean bottom. Figures 1 and 2 show computed TKE and TKE dissipation respectively 10 000 m downstream near the ocean bottom at the end of the second day for Case 1 (non-stratified case). Immediately above the ocean bottom, TKE and TKE dissipation are the greatest because of the steep velocity gradient enhancing TKE production. While TKE dissipation rapidly reduces in magnitude, TKE is almost uniform from several metres to 45 m above. The sharp reduction in TKE above 45 m results because the vertical gradient of the calculated longitudinal velocity above 45 m becomes very small (i.e. the longitudinal velocity above 45 m reaches its uniform velocity value of 0·1 $m\ s^{-1}$); thus there is no shear production of TKE due to the velocity gradient.

Cases 2 and 3 (stratified cases) reveal the suppression effects of the density gradient on TKE production. These effects are especially strong for Case 3, which has the density gradient near the bottom (6·0–7·5 m above the bottom) where the vertical velocity gradient is steep. Figures 3 and 4 show computed TKE and TKE dissipation for Case 3, indicating reduced TKE and TKE dissipation values as compared to those of Case 1 (Figures 1 and 2). Figures 5 and 6 show calculated eddy viscosity distributions (from equation (1)) based on k- and ε-values shown in Figures 1–4. Both figures reveal that the eddy viscosity increases almost linearly with vertical distance just above the ocean bottom. After reaching their maximum values near the ocean bottom, predicted eddy viscosity values reduce rapidly to almost molecular viscosity values with vertical distance. The calculated maximum eddy viscosity value after two days of simulation for Case 1 (non-stratified case) is approximately 20 Pa s (or 200 $cm^2\ s^{-1}$), occurring around 30–45 m

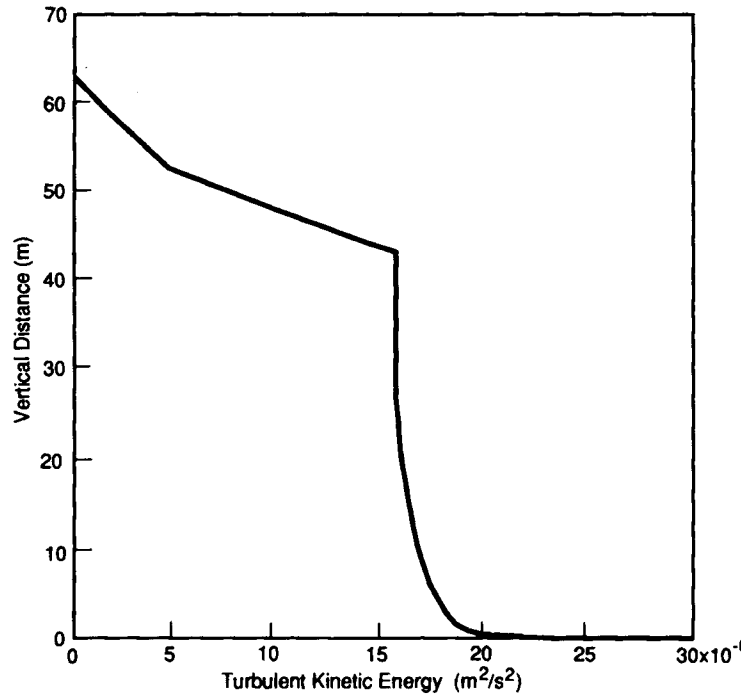

Figure 1. Vertical distribution of calculated turbulent kinetic energy near the ocean bottom for the non-stratified Case 1

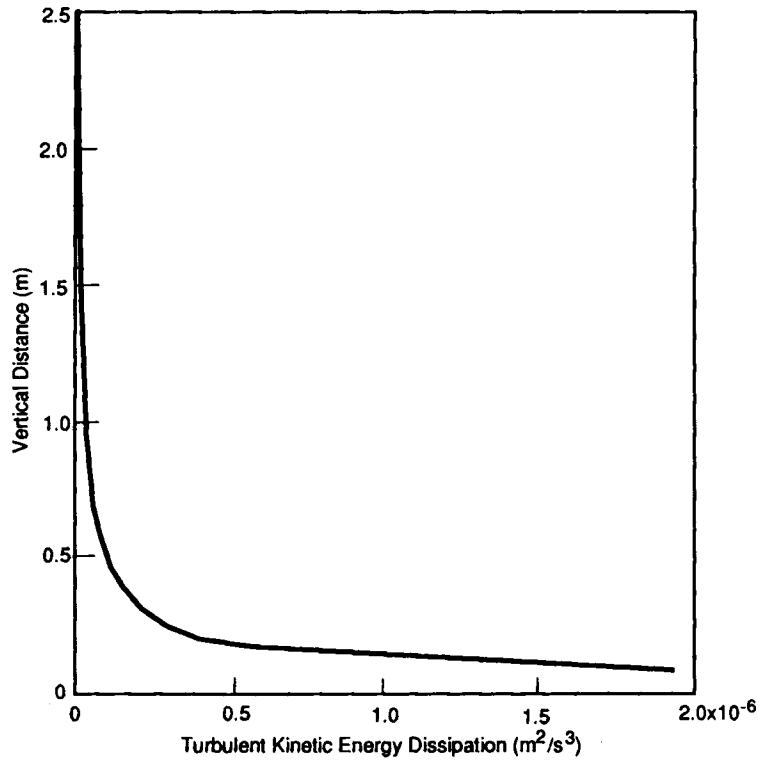

Figure 2. Vertical distribution of calculated turbulent kinetic energy dissipation near the ocean bottom for the non-stratified Case 1

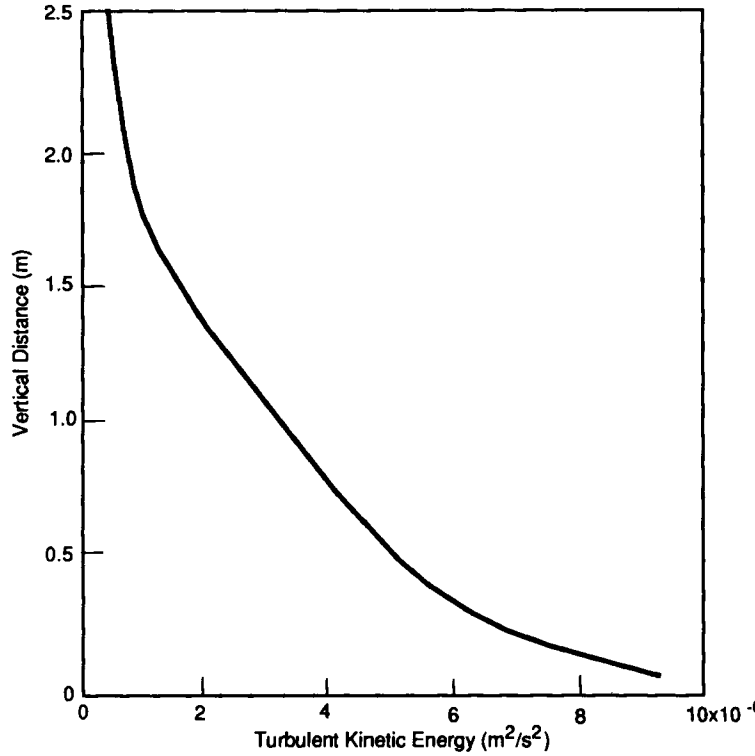

Figure 3. Vertical Distribution of calculated turbulent kinetic energy near the ocean bottom for the stratified Case 3

above the ocean bottom, while the maximum value of 0·2 Pa s (or 2 $cm^2 s^{-1}$) occurs 1 m above the bottom for Case 3 (near-bottom stratified case). The significant reduction in eddy viscosity value for Case 3 as compared to Case 1 is caused by the density gradient near the ocean bottom, where production and dissipation of TKE are the greatest; thus the density gradient causing reduction in TKE production there affects these values significantly. The calculated eddy viscosity of 2 $cm^2 s^{-1}$ for Case 3 agrees well with the vertical eddy diffusivity of 1 $cm^2 s^{-1}$ reported by USAEC,[10] shown in Table III. Note that we have reported eddy viscosity values in Table III from the reported eddy diffusivity values and an assumed Prandtl or Schmidt number of 0·7. Furthermore, the high eddy diffusivity and eddy viscosity values in the surface layer reported in Table III are caused by wind shear and other near-surface processes which this study did not consider.

Case 2 (not-near-bottom stratification case) has the computed maximum eddy viscosity value of 17 Pa s (170 $cm^2 s^{-1}$), occurring 45 m above the bottom. Since Case 2 has the density gradient occurring 120–150 m above the ocean bottom, the calculated longitudinal velocity did not become uniform until approximately 250 m above the bottom. This resulted in more gradual variations of TKE and eddy viscosity values in the bottom 70 m area and little reduction of TKE and eddy viscosity values from Case 1 (non-stratified case).

The velocity distributions for all these cases showed fully developed profiles. However, Cases 1 and 2 showed well-developed, flattened velocity profiles, while Case 3 showed more parabolic profiles, reflecting smaller eddy viscosity values for this case.

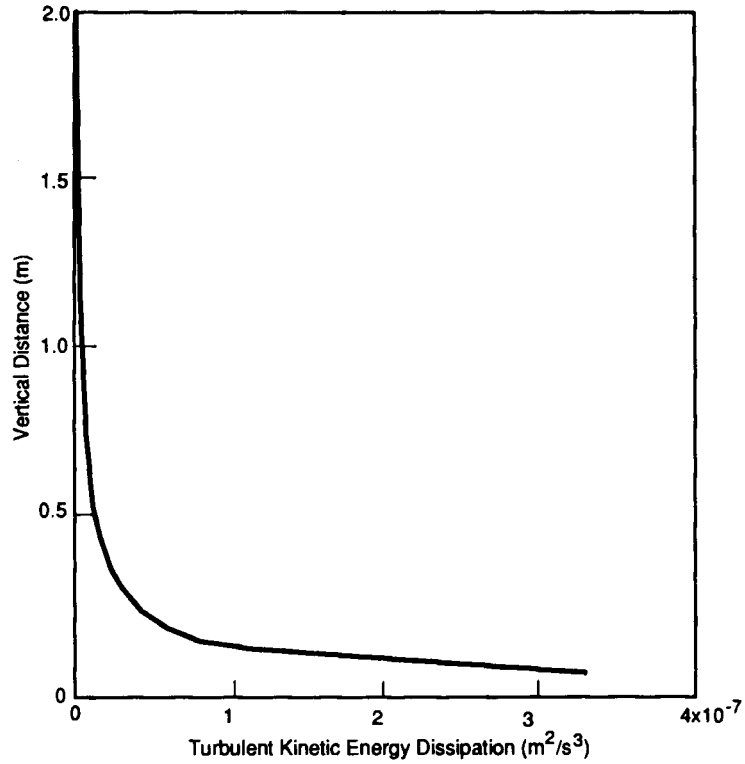

Figure 4. Vertical distribution of calculated turbulent kinetic energy dissipation near the ocean bottom for the stratified Case 3

The turbulence-modelling results indicate that the k–ε model produced qualitatively reasonable eddy viscosity distributions, especially for Case 3 conditions.

Sediment and radionuclide modelling

Computed quasi-steady state eddy viscosity values were imposed as input to the FLESCOT model to predict distributions of radionuclides originally disposed on a small portion of the ocean bottom. Because of the very small vertical grid spacing near the ocean bottom with the total water depth of 3000 m, the 0·1 s time step was used to avoid the numerical instability. The calculated results are those obtained after 6 h; thus the radionuclide concentrations have not reached a final steady state yet.

The model predicted that a small portion of the radionuclide sorbed by the bottom sediment leached out to the overlying water. Once in the water column, dissolved radionuclides leached out from the ocean bottom were then transported downstream by the current, as shown in Figure 7. Moreover, some of them were then adsorbed by suspended sediments (i.e. silt and clay), as shown in Figure 8 for the computed radionuclide adsorbed by suspended silt. The model predicted that the ratio of the concentrations of the radionuclide sorbed by suspended silt and clay is equal to the ratio of the distribution coefficients associated with silt and clay. As shown in Figure 9, the originally clean bottom sediments downstream of the contaminated bottom portion (the

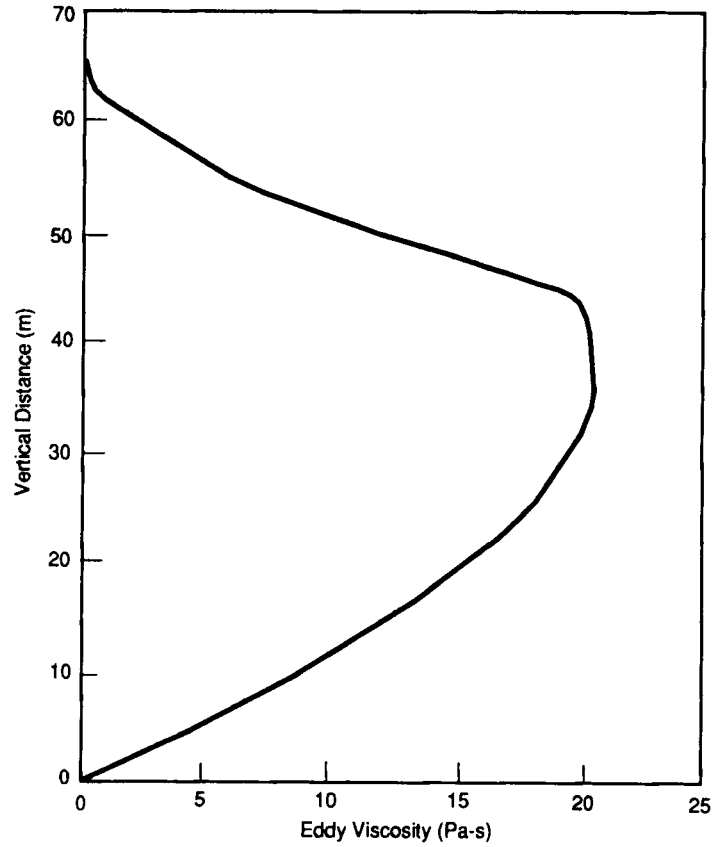

Figure 5. Vertical distribution of calculated eddy viscosity near the ocean bottom for the non-stratified Case 1

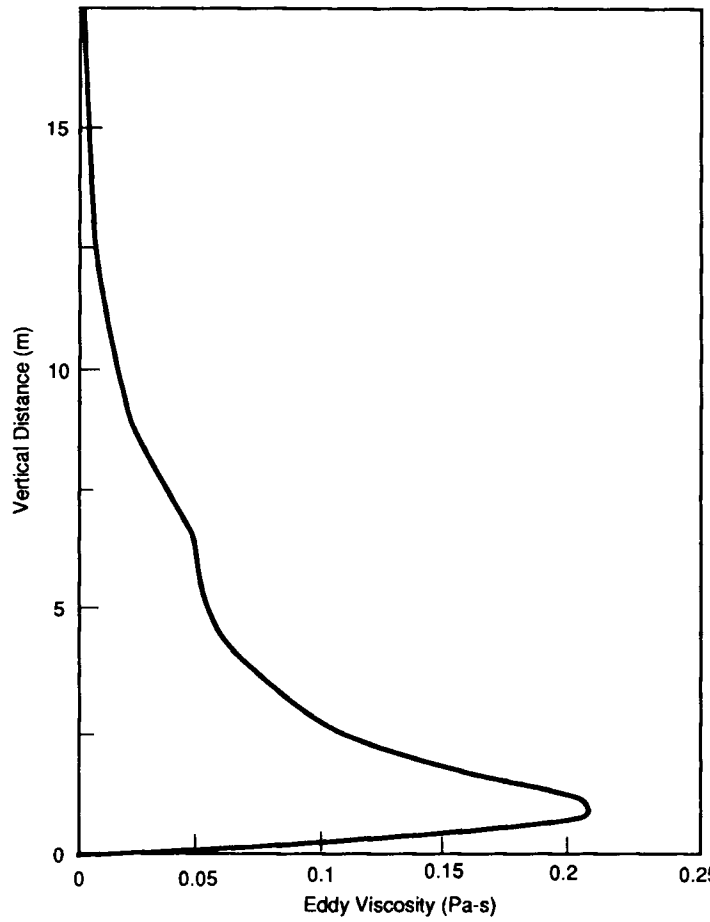

Figure 6. Vertical distribution of calculated eddy viscosity near the ocean bottom for the stratified Case 3

Table III. Variations in eddy diffusivity and viscosity[10]

Layer	Depth (m)	Vertical eddy diffusivity ($cm^2 s^{-1}$)	Estimated eddy viscosity ($cm^2 s^{-1}$)
Surface	75	50·0	35·0
Intermediate	500	0·1	0·07
Deep	2000	1·0	0·7

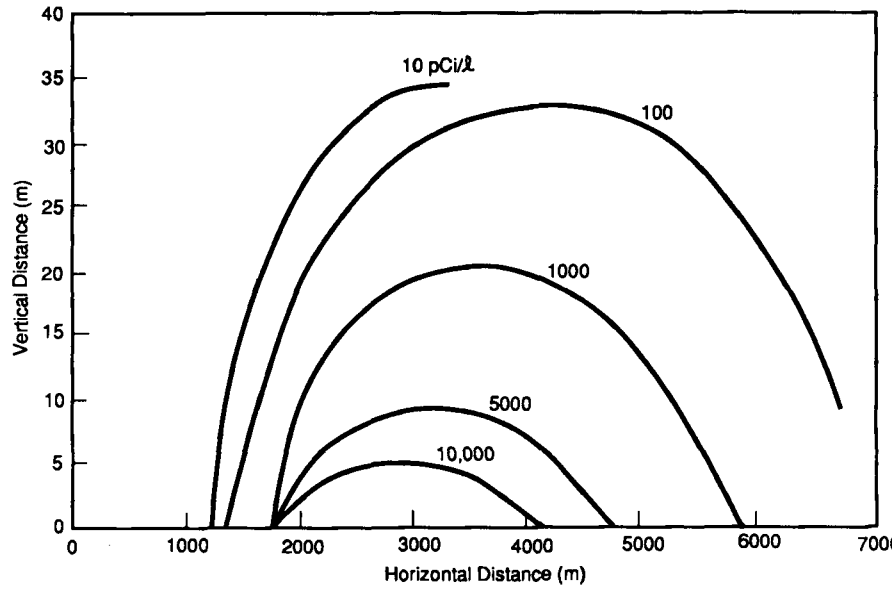

Figure 7. Calculated dissolved radionuclide concentrations near the ocean bottom for the non-stratified Case 1

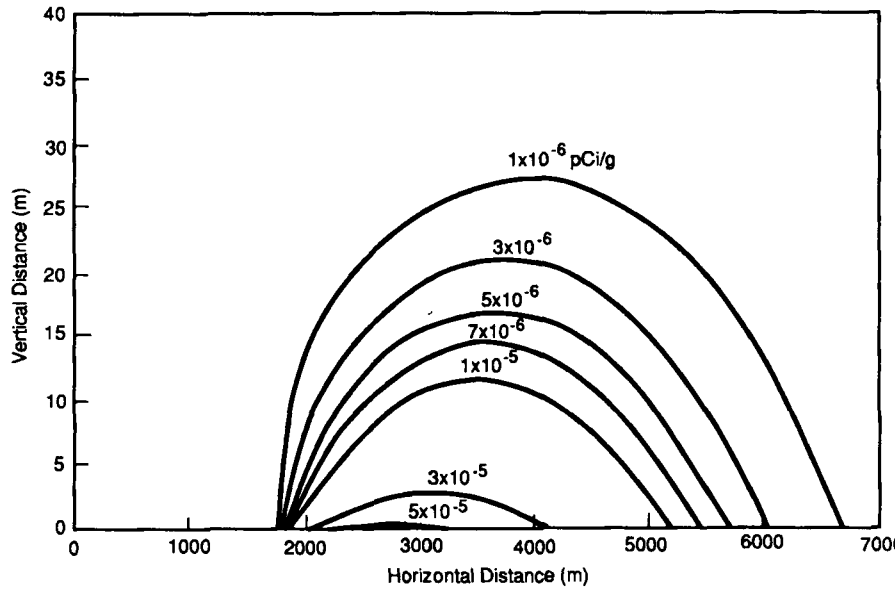

Figure 8. Calculated suspended-silt-sorbed radionuclide concentrations near the ocean bottom for the non-stratified Case 1

1500–2000 m portion) then adsorbed a fraction of the radionuclide in the water column back into the ocean bottom, thus further spreading the long-term contamination source in the ocean. Because there are no data to be compared, these model results should be regarded as strictly qualitative. Nonetheless, these results depicted reasonable pictures of potential radionuclide migration patterns.

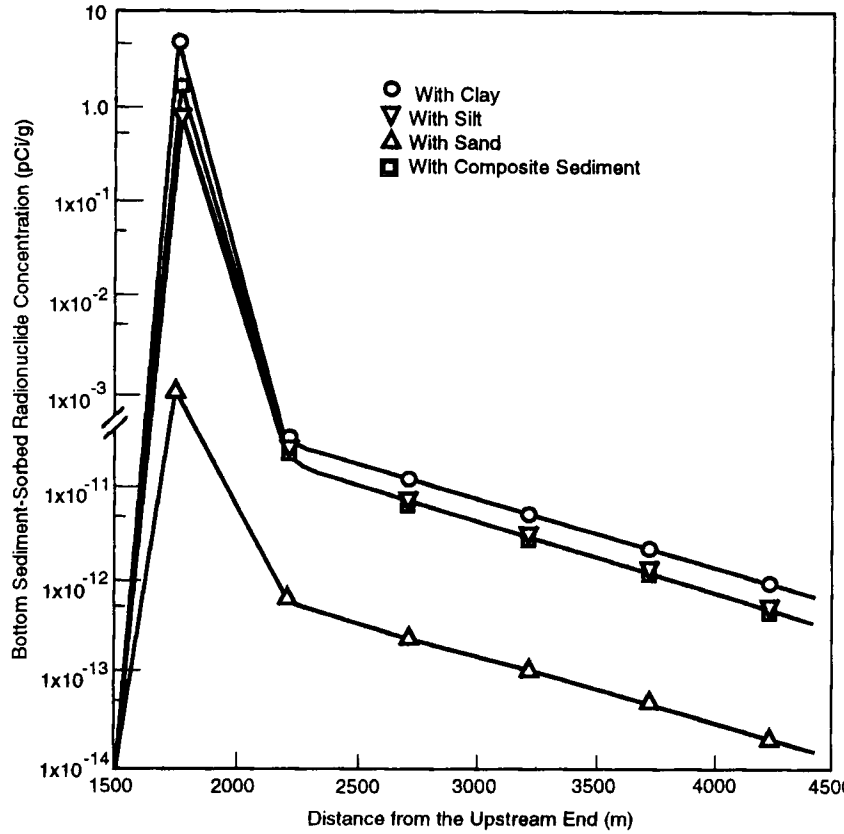

Figure 9. Calculated radionuclide concentrations sorbed by bottom sediments in the top 3 cm bed layer for the non-stratified Case 1

CONCLUSIONS

The TEMPEST and FLESCOT models with the k–ε turbulence model simulated hypothetical flow, turbulence, water temperature and sediment and radionuclide distributions in the deep ocean environment. The model results demonstrated that the density gradient to suppress TKE production must be considered for the eddy viscosity calculations, as demonstrated by the close match of computed, 0·2 Pa s (or 2 $cm^2 s^{-1}$), and reported, 0·07 Pa s (or 0·7 $cm^2 s^{-1}$), eddy viscosity values for Case 3 (near-bottom stratification case). These results indicate that the k–ε turbulence model qualitatively reproduced the vertical eddy viscosity variations occurring near the bottom. Further detailed modelling should be conducted to quantitatively evaluate the adequacy of the k–ε model to confirm this tentative conclusion, as well as effects on the dynamic and hydrostatic pressure computations of the turbulence structures.

ACKNOWLEDGEMENTS

This work was supported by the U.S. Environmental Protection Agency under a Related Services Agreement with the U.S. Department of Energy (DOE) under Contract DE-AC06-76RLO 1830,

Interagency Agreement DW90059-01. Pacific Northwest Laboratory is operated for the DOE by Battelle Memorial Institute.

REFERENCES

1. Y. Onishi, L. F. Hibler and C. R. Sherwood, 'Review of hydrodynamic and transport models and data collected near the mid Atlantic low-level radioactive waste disposal sites', *PNL-6331*, Pacific Northwest Laboratory, Richland, WA, 1987.
2. Y. Onishi, D. S. Trent and A. S. Koontz, 'Three-dimensional simulation of flow and sewage effluent migration in the Strait of Juan De Fuca, Washington', *Proc. ASCE Environmental Engineering Conf.*, Boston, MA, 1985, pp. 1006–1013. ASCE, New York, 1985.
3. Y. Onishi and D. S. Trent, 'Three-dimensional simulation of flow, salinity, sediment and radionuclide movements in the Hudson River estuary', *Proc. ASCE Hydraulics Division Conf.*, Lake Buena Vista, FL, 1985, pp. 1095–1100. ASCE, New York, 1985.
4. W. Rodi, 'Examples of calculation methods for flow and mixing in stratified fluid', *J. Geophys. Res.*, **92** (C5), 5302–5328 (1987).
5. E. Partheniades, 'A study of erosion and deposition of cohesive soils in salt water', *Dissertation*, University of California, Berkeley, CA, 1962.
6. R. B. Krone, *Flume Studies of the Transport of Sediment in Estuarial Shoaling Processes*', Hydraulic Engineering Laboratory and Sanitary Engineering Research Laboratory, University of California, Berkeley, CA, 1962.
7. V. A. Vanoni (ed.), *Sedimentation Engineering*, American Society of Civil Engineers, New York, 1975, pp. 191.
8. W. D. Grant and O. S. Madsen, 'Combined wave and current interaction with a rough bottom', *J. Geophys. Res.*, **84**, (C4), 1797–1808 (1979).
9. A. A. Amsden and F. H. Harlow, 'The SMAC method: a numerical technique for calculating incompressible fluid flows', *LA-4370*, Los Alamos National Laboratory, Los Alamos, NM, 1970.
10. U.S. Atomic Energy Commission, *Overall Safety Manual*, Vol. 2, Space Nuclear Systems Division, Washington, DC, 1975.